Hindawi
Journal of Engineering
Volume 2023, Article ID 2420903, 13 pages
https://doi.org/10.1155/2023/2420903

Research Article

Plug Valve Surface Defects Identification through Nondestructive Testing and Fuzzy Deep-Learning Algorithm for Metal Porosity and Surface Evaluation

V. Jacintha,[1] **S. Karthikeyan**,[1] **and P. Sivaprakasam**[2]

[1]*Department of Electronics & Communications Engineering, Sathyabama Institute of Science & Technology, Chennai, India*
[2]*Department of Mechanical Engineering, College of Electrical and Mechanical Engineering, Addis Ababa Science and Technology University, Addis Ababa, Ethiopia*

Correspondence should be addressed to P. Sivaprakasam; shiva@aastu.edu.et

Received 7 July 2022; Revised 24 July 2022; Accepted 26 July 2022; Published 27 March 2023

Academic Editor: Karthikeyan Sathasivam

This paper addresses the detection and identification of flaws in Plug valves. The Plug valve thermal image is acquired using a Fluke thermal camera [TiS20]. Thermal images of the Plug valve are used for the identification of flaws such as Crack, Porosity, Corrosion, and Internal defects. The thermal images detect the surface flaws and never subsurface flaws in Plug valves. The subsurface flaws detection is a challenging problem in valve inspection. In this paper, the thermal images obtained after the dye penetrates the surface valve detect the surface flaws more efficiently after applying the Fuzzy Deep Learning Algorithms. DyePenetrating Test (DPT) combined with Infrared Thermography is proposed to identify heat flux changes and flaws in the faulty metal surface of Plug valves. In DPT, thinned paint is employed on the metal surface that displays metal porosity and even fine cracks. After DPT, thermal images of the Plug valve are processed through the Fuzzy Deep Learning Algorithm to evaluate flaws. The Fuzzy Algorithm is utilized prior to Deep Learning to simplify and speed up the classification task. The flaws are identified using Slicing operation and the following parametric quantities such as Accuracy, Mathew's Correlation Coefficient (MCC), Local Self-Similarity Descriptor (LSS), Precision/Recall, *F*-measure, and Jaccard Index. The parametric quantities depict corresponding variations with regard to surface coarseness and metal flaws. The DPT and Fuzzy Deep Learning Algorithm identify metal defects with 80.67% accuracy.

1. Introduction

The American Petroleum Institute (API) criterion encompasses inspection, examinations, and pressure test for metal-to-metal seated Plug valves. The manufacturer and purchaser perform the inspections. The inspection may include a pressure test conducted in manufacturer's plant. During assembling of Plug valve components, inspection is done through Nondestructive Testing (NDT). The valve manufacturer initially performs a Dye-penetrating examination. Furthermore, liquid penetrant testing is performed according to American Society of Mechanical Engineers (ASME) *B* 16.34 standards. Moreover, Pressure test is accomplished with any external pressure due to seat leakage. Moreover, when an end-clamping fixture is used, it does not affect the seat leakage of the Plug valve. For lubricating Plug valves, high-pressure closure test is compulsory while low-pressure closure test is an option. Furthermore, Backseat test is required for Plug valves and a High-pressure pneumatic shell test is very important for Plug valve inspection. The pressure during testing will be 110% of maximal permissible pressure at 100 F (38°C). The test fluid used for a high-pressure test can be air, inert gas, kerosene, water, or noncorrosive liquid with a viscosity lesser than that of water. The test fluid temperature range shall be within 41 F (5°C) to 122 F (50°C). For low-pressure test, the test fluid can be air or inert gas. These test fluids detect any leakage in the valve. Water utilized for any test may comprise of water-soluble oil or rust inhibitor. A wetting agent may also be included in water. Plug valves are generally made of cast iron or stainless

steel, and for these materials water having a chloride capacity within 100 parts/million (ppm) can be utilized. For Shell tests and Backseat tests, a visually detectable leakage is not permitted from any part of the valve. For valves with adjustable steam seals, the manufacturer must look for steam seals, which are capable of retaining pressure of at least 100 F (38°C) valve grading free from visible leakage. For valves, with nonadjustable steam seals, a visually noticeable leakage throughout the shell test is not permitted. If the test fluid is liquid, there shall be no seeable proof of droplets or wetting of the outside surface of the valve. If the test fluid is air/inert gas, no leakage will be revealed by the detection procedure. For both low-pressure and high-pressure closure tests, it is not permitted to have any visual evidence of leakage as well as any structural damage anywhere in the Plug valve. Recently, quality inspection of material has been automated for increasing productivity with a quality-finished product. The automation process reduces the manual inspection because of sleek design and functionality of automated machines. The automated machines for material quality inspection perform better than manual inspection. The automation processes detect faults in a material more accurately and classify their quality level. The main advantages of automated inspection over manual processing are 24/7 operation, high speed, continuous monitoring with remote access through sensors, and working with different kinds of materials. The component in an automated inspection system consists of control circuits, sensors, image acquisition system, and image-processing algorithms for zero defects in the production unit. The automation process of inspection starts with an image acquisition of the material under inspection through machine-vision cameras. The machine-vision camera captures the images of materials, transmits them to the computer for image analysis, and decides the quality based on image-processing algorithms. Three parameters that need to be taken into account while setting the camera and lens during image acquisition are the viewing angle, depth of field, and target area [1]. The image-processing algorithms is used for detect flaws in the Plug valve material. The Plug valve needs critical inspection during the manufacturing process to avoid repairs and failures. The critical inspection prevents external and internal leakage in oil and gas applications. Figure 1 shows the line diagram of a Plug valve. In oil and gas applications, surface defects will grow exponentially because of cavitations, high velocities, high-pressure drops, throttling, and solids/slurries. The root cause of all these problems mentioned is solved through an automatic inspection system over the valve surface. However, the existing automatic inspection system is performed with machine-vision cameras or ultrasonic surface crack detection. The vision-based quality inspection systems analyze the surface of a Plug valve without injection of the test fluid. The ultrasonic surface crack detection testing also cannot analyze the surface during test pressure and test leakage. The solution for surface analysis in a Plug valve is performed with ultrasonic surface crack detection and Dye-Penetrating test. The Plug valve surface testing of the test fluid under pressure through thermal vision automatic inspection system identifies the various defects on the inner surface of Plug valves. Infrared Thermography renders enhanced solutions for online identification of Internal defects [2]. The various defects on the surface, such as Cracks, Porosity, Internal defects, and Corrosion, are identified before and after the test fluid inspection is completed. These flaws are the cause for initial fatigue crack initiation (FCI) and should be reduced to enhance the fatigue life of a weld joint [3]. The investigation strongly detected the location and type of flaws [4].

Figure 1: Plug valve with inverted plug type design.

The surface valve defects identified through the thermal images before and after the fluid test analyze the surface temperature during high pressure. It is necessary to acquire thermal images over the inner and outer surfaces of the Plug valve and study surface characteristics in terms of Cracks, Porosity, and Internal defects. Porosity defects can be easily eliminated in the presence of vacuum [5]. Furthermore, images acquired after certain duration of time are used to check the corrosion on surface, once the complete testing of valves is finished. These acquired thermal images under different faults are trained using Deep Learning algorithms after images are processed through Fuzzy Cluster algorithms. The applicability and novelty of the proposed work are given in Table 1.

2. Literature Survey

2.1. Inferences from Literature Survey. From the review of literature till now, the various faults are identified using a high-speed camera, signal processing and soft computing algorithms such as wavelet transform, genetic algorithm, and neural network. However, these tests were conducted only in offline mode, i.e., the materials were tested without test fluids, especially in valves. Plug valves being the most frequently utilized valves are primarily used in oil and gas industries, and require multiple inspections on the surface of the valve. In the existing system, the Plug valve is examined using the Dye-Penetrating test, Ultrasonic test, and Fluid test. These testing methods are performed independently in offline mode. Using Nondestructive Testing (Dye-Penetrating Test), we can identify the surface defects such as Cracks. To identify the subsurface defects such as Porosity and Internal defects, we utilize Ultrasonic Nondestructive Testing. Using Nondestructive Testing, we can only detect

Table 1: Applicability and novelty of the proposed work.

Technique	Applicability	Remarks
Machine learning [6]	Difficulty for real-time application	Nonavailability of real-time datasets for implementation. Learning process is slow, with issues in reusing, integrating, and debugging the models.
Neural network [7]	Not applicable	The training time is quiet long. There are chances for misclassification to occur.
Deep learning	Applicable	Automated feature extraction and classification. Training time is less with no misclassifications. Works effectively on real-time plug valve images.

the Plug valve defects; however for defect classification, we require a combination of the Fuzzy Slicing Algorithm and the Deep Learning Architecture. A novel method of combining these methods is required to improve the accuracy in testing with low cost and reduce the time in a single test. The various research work related defect detection is presented in Table 2.

3. Materials and Methods

The Plug valves classify as Lubricated and nonlubricated design along with varied port openings, single and multiple port plugs. The Plug valve is used under great pressure and extreme temperature. The Plug valves are prone to defects such as Cracks, Porosity defects, Internal defects, and Corrosion. Among these flaws, Cracks are the major problem, which is to be identified at the early stage, or otherwise it would lead to rework and consume more time. Miniature Crack is a line on the surface of the valve and later causes fragments, which lead to a serious damage. These miniature cracks are not able to be visualized through human eye and become visible only after certain duration once the Plug valve undergoes heavy testing. The major cause of these cracks because of tension in the Plug valve becomes greater than the metal strength. When the heavy pressure works on Plug valves, the stress develops and it accumulates. The Porosity occurs over the welded regions in the Plug valve. This porosity forms due to trapped or shielding gases and pressure on welded specimen is produced. The gases are engulfed in the liquefied specimen and later expelled on the welded metal after solidification. If the porosity is in the form of round holes then it is called as spherical porosity, but when the holes are stretched the flaws are called as wormholes or piping. Corrosion occurs in the Plug valve metals after reacting with the ambient temperature and atmosphere. The corrosion occurs due to electrochemical oxidation because of the Plug valve metal surface reacting with oxygen or sulfate present in the atmospheric gases. The Internal cracks occur in the Plug valve in the inner surface of the welding regions. The two types of welding metal cracks are Root cracking and heat-affected-zone (HAZ) cracking (under bead cracking). Weld metal cracks are flaws that occur within the liquefied metal. HAZ cracks are flaws that occur when the weld solidifies at a very fast rate, which makes the base material to be very fragile, thereby resulting in internal cracks. Gas porosity types such as Pinholes, Subsurface Blow holes, and open holes are used. Pinholes alias porosities are below 2 mm hole size and present in molds of upper surface. Subsurface blowholes' size is of more than 2 mm in diameter, which occurs inside the cast and seeable only after prolonged usage of the valve. The open holes occur during casting and the surfaces hence are easy to detect. Cracks in valves classify into two types such as hot cracks and cold cracks. The hot cracks happen because of crystallization procedure in the weld joint. Cold cracks form after welding, when the weld happens to cool down. The solids or slurries of abrasive nature gradually wear down from the Plug valve surface. The cavity flaws caused when the pressure inside the valve falls drastically below the vapor pressure lead to vapor bubbles. When the pressure is low in valves, these bubbles burst causing dents onto the metal surfaces which gradually wear down the valve body, resulting in an abnormal noise during operation, and which reduce the flow rates in the valves.

3.1. Detection of Plug Valve Defects through Thermal Images. Plug valve defects are detected through thermal images acquired during the testing conditions such as Pressure test and Dye-penetrating method. Figure 2 shows the block diagram of Nondestructive Testing of a Plug valve through thermal imaging. Thermal images are acquired from a Plug valve for defect identification using Fluke thermal camera (Model No: TiS20). The thermal camera consists of a 5 hrs battery life. The camera works on Passive Infrared Thermography principle and never requires an external energy source. Infrared thermography camera detects infrared radiation emitted from an object and converts it into temperature for thermal image. The optics of the thermograph enables the rays to concentrate on the thermal detector and produces an image directly proportional to the radiation. The thermal camera needs less maintenance and is easy to operate. The thermal images are acquired for defects' detection from the images taken before and after, Pressure test and Dye-Penetrating test. Pressure test: In a Plug valve, the test fluid is liquid; the valve must be necessarily free from entrapped air throughout the test. Furthermore, safety coatings on the valve surface should be strictly avoided before pressure test, since they cover the surface defects. Dye-Penetrating inspection (DPI) works on the principle of Capillary action. In a DPI method, thin liquid sinks into a clear and dry surface and goes into the flaws and thereby makes flaws clearly visible. For the DPI method, the items such as cleaner, penetrant, and developer are required. Initially, the inner surface of a Plug valve is cleaned and impurities removed for applying the penetrant and developer. Next, the penetrant is sprayed over the inner surface of the Plug valve using a brush. The penetrant, which is surplus

Table 2: Recent research work related to defect detections.

Author/Year	Problem	Solution
Ye and Toyama [6]	To analyze the efficiency of various deep learning architectures.	A total of 7000 real-time images are evaluated. A total of 17 flaws are detected.
Ajmi et al. [8]	Defect detection and classification on small weld X-ray image datasets.	Data augmentation and deep learning techniques utilized for obtaining best results.
Mery [7]	To automate the process of defect detection in aluminum castings.	Convolution neural network (CNN) model utilized for effective detection of defects
Daniel et al. [1]	Internal defects in pipes (0 to 2 inches).	Vertical insertion camera.
Xiao et al. [9]	To detect weld bead width and depth of penetration defects in welds.	Coaxial infrared pyrometer
Schaunberger et al. [10]	To identify weld seam defects such as pores, tapers, and regressions (copper)	Defect detected from temperature curves.
Gao et al. [11]	Process stability and weld formation (laser welding)	Analysis with a high-speed camera.
Lei et al. [12]	Influence of thermal effect on droplet transfer (cold metal transfer (CMT) laser welding)	Analysis with a high-speed camera and brightness curves
Huang et al. [13]	Welding defect identification (laser welding)	The defect identification through electrical signals of laser plasma and plasma flumes acquired by a high-speed camera
Gao et al. [14]	To identify invisible weld defects	Magneto-optical imaging system and grayscale curves
Hamade and Baydoun [4]	To identify wormhole defects in welded lap joints.	X-ray computed tomography (CT) scan and Otsu segmentation
Zhang et al. [2]	To detect weld seam penetration defects	Multiangle image acquisition and convolution neural network (CNN)
Jiang et al. [5]	To identify porosity defects at ambient pressures.	High-speed camera. No defects under vacuum
Xie et al. [15]	To detect metal rust	High-speed images and Acoustic emission signal of pulsed laser
Zhou et al. [16]	To identify surface pit, spatter, softening in heat-affected zone (HAZ), oxide, and porosity	Addition of Sn foil
Choi et al. [17]	To detect lack of fusion (LOF), gas pores	Laser metal deposition technique and fatigue test to check efficiency.
Bacioiu et al. [18]	To monitor tungsten inert gas welding	High dynamic range camera and Fully convolution neural networks and convolution neural networks (FCN & CNN).
Shah and Liu [19]	To identify interfacial cracks, solidification cracks, surface defects, and oxides	Ultrasonic waves in resistance spot welding (URSW)
Nacereddine et al. [20]	To detect cracks, porosity, lack of penetration (LOP), and solid inclusion	Classification in radiographic images.
Francis et al. [21]	To analyze the potential of vacuum laser welding for thicker areas of nuclear parts.	Achieves the required weld quality equivalent to the electronbeam welding (EBW).
Zhang et al. [22]	Comprehensive insights of laser welding process.	Multiple optical sensor systems
Xu et al. [23]	To identify Keyhole-induced porosity	Three-dimensional transient model
Chaoudhuri et al. [3]	To identify Inherent flaws and fatigue cracks	Stress analysis and micro-computed tomography (CT)
Son et al. [24]	To examine the strength that exists between a material deposited and its substrate.	High bonding strength verified through Shear tests.
Reisgen et al. [25]	To detect porosity defects	)Nonvacuum electron beam welding (NV-EBW)
Millon et al. [26]	To identify the lack of fusion (LOF) or porosity defects	Laser ultrasonic signals.
Wu et al. [27]	Expulsion identification	Welding force signal
Xie et al. [28]	Heat-affected zone (HAZ) Cracks(liquidation and strain age cracks)	Postweld hot isostatic pressing
Qian et al. [29]	To identify high residual stress	Spontaneous magnetic signals
Kim et al. [30]	To detect welding defects in underground curled pipelines	Magnetic flux leakage (MFL) sensor signals
Hongmin and Wang [31]	To identify tiny weld bead flaws (cracks, pores, lack of fusion (LOF), cavities)	Closed magnetic reluctance signals
Zhang et al. [32]	To detect flaws in power disk laser welding	Spectrometer signals
Li and Lu [33]	To fetch a novel alloy for Biomedical utilization with the apt Young's modulus	Powder metallurgy procedure is employed.
Proposed system	To identify porosity, crack, internal defects, and corrosion	Thermal images and fuzzy deep learning algorithm

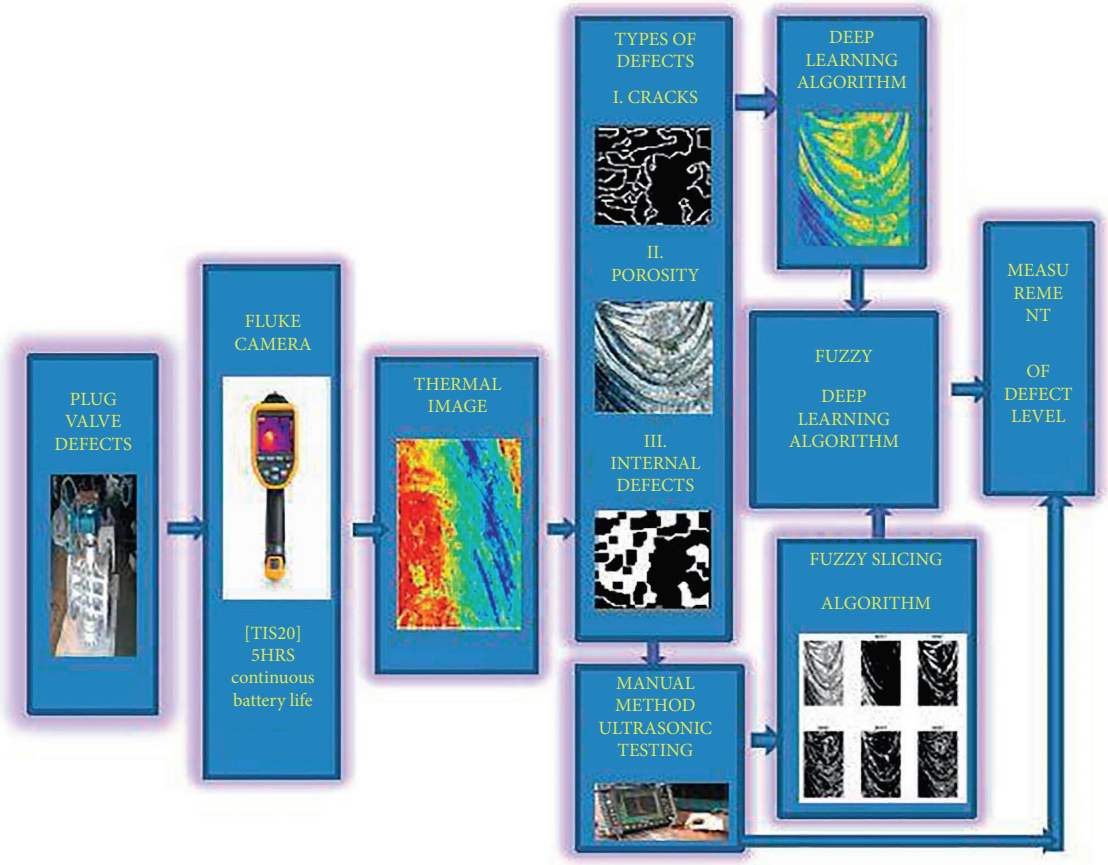

Figure 2: Block diagram of the proposed system.

over the Plug valve surface, is removed using cotton. Next, the developer is applied to make the flaws visible to naked eye. Furthermore, after visible inspection thermal images are obtained from the valves to detect the invisible flow using the proposed algorithm.

3.2. Ultrasonic Inspection. The Ultrasonic testing is performed through a SUB280 model instrument. The instrument consists of the following sections, Ultrasonic sensor and secure power supply unit with power barrier, signal barrier, RS485/RS232 converter, and Leak supervising software. The instrument checks the surface of the Plug valve for leakage using Acoustic emission. The Acoustic emission of the surface of the Plug valve reflects the distorted amplitude from the leakage surface. The leakage surface noise and the fluctuating amplitude show the change in pressure field linked with the flow of liquid in unstable condition. The instrument tracks the leakage for cylindrical surface in the Plug valve and the detection of minute leakage is still a challenging problem. For detecting the minute leakage, the thermal images are obtained for analysis through the proposed system.

3.3. Fuzzy. Fuzzy logic is performed through logical thinking with membership rules and functions. Fuzzy logic provides an effective solution for complex problems, with high accuracy and speed in execution. Fuzzy has a wide range of degrees of membership between 1 and 0. The partial membership arises when an element of one fuzzy set belongs to the other fuzzy set in the sample space. Fuzzy logic method is highly desirable for unsure or estimate reasoning with equivocal boundaries. Fuzzy logic algorithm is applied in image processing to resolve uncertainty issues in image pixels. Fuzzy logic finds the differences in the image pixels, which are either true or false, for a set of pixels. The Fuzzy logic is applied in the thermal image of valves to detect the faults in the valves. Fuzzy logic combines with Deep Learning techniques for fault detection. Fuzzy clustering permits the information to be grouped in greater than one cluster. The membership function (μ_{mn}) denotes the membership degree, as to which mth cluster the nth object belongs to.

The aim of the algorithm is to reduce the cost function, given as.

$$D = \sum_{n=1}^{N} \sum_{m=1}^{C} \mu_{mn}^{l} i_n - v_m^2, \tag{1}$$

N denotes the objects to be labeled (i.e., count of the image pixels). C denotes the cluster count. v_m represents the mth cluster centroid ranging from $\{v_1, v_2, \ldots, v_m\}$. l denotes the parameter that controls fuzziness that should be greater than 1. i_n denotes the particular image pixel. $\|\cdot\|$ represents the Euclidean distance measure. The cost function is minimized by continuously updating μ_{mn} and v_m.

$$\mu_{mn} - \frac{i_n - v_m^{-2(l-1)}}{\sum_{k=1}^{C} i_n - v_k^{-2(l-1)}},$$
$$v_m = \frac{\sum_{n=1}^{N} \mu_{mn}^{l} i_n}{\sum_{n=1}^{N} \mu_{mn}^{l}}. \quad (2)$$

The general fuzzy c-means (FCM) never considers any spatial information, therefore it is hindered by noise and artifacts. Hence, Spatial Fuzzy Clustering along with level set segmentation is considered for automated segmentation of defects in Plug valve images. Initially, Spatial FCM integrates spatial data throughout an adaptive optimization that obviates the intermediary morphological functions. The controlling parametric quantities required for Level set segmentation are obtained directly from the outcome of Spatial FCM. Finally, the Spatial FCM regularizes the Level set function.

The Level set function is denoted as,

$$\phi_0(x, y) = -4\varepsilon(0.5 - B_k), \quad (3)$$

where ε is a constant quantity governing the Dirac function. The Dirac function is expressed as:

$$\delta_e(x) = \begin{cases} 0, & |x| > \varepsilon, \\ \frac{1}{2\varepsilon}\left[1 + \cos\left(\frac{\pi x}{\varepsilon}\right)\right], & |x| \le \varepsilon. \end{cases} \quad (4)$$

B_k denotes the binary image expressed as $B_k = R_k \ge b_0$. Where b_0 is an adjustable threshold value. R_k denotes the region of interest in the FCM outcome.

3.4. Deep Learning. Deep learning is the part of machine learning and solves the problem like human brain, much better than human brain. Deep learning structure is similar to neural network, so called deep learning neural network. Neural network can go for two hidden layers, whereas Deep learning can go for 128 layers. Deep learning needs large datasets and specialized hardware such as graphics processing unit (GPU). However, machine learning needs less number of datasets and never needs any specialized hardware. The accuracy of Deep learning is better than those of machine learning and neural network. In Deep learning, computers learn to carry out classification straightaway from images, text, or sound. Deep learning does the same job many times and learns. The learning process in Deep learning is obtained from vast unstructured, interconnected datasets and from the learning solves the problem. Deep learning in image processing is utilized for object recognition, classification, and segmentation. In object recognition, Deep Learning algorithm can locate the object in the image, even in multiple locations without human intervention. Deep Learning algorithm detects faults in a Plug valve. Deep Learning algorithm classifies the defects in low-quality images. The Deep Learning algorithm is able to detect the various faults such as Porosity, Corrosion, Internal defects, and Cracks and multiple defects in single region. Recurrent Neural Network (RNN) is a type of Neural Network in which the output from the current step is fed as input to the next step; hence, it does not have the necessity to remember the outcomes of every step. The unique characteristics of the RNN are the Hidden State that has the capability to store and retrieve data in a sequence or operation. It utilizes common parametric quantities for all the inputs, since it executes a similar operation for all the inputs or hidden layers to yield the output. It renders common weights and biases to all layers, thereby lessening the issue of handling more parameters. Hence, these three layers can be merged together into a single recurrent layer. In this paper, RNN is utilized for fault detection.

The current state is expressed as follows.

$$h_t = f(h_{t-1}, x_t), \quad (5)$$

here, h_t is the present state, h_{t-1} is the former state while x_t is the present input. The input neuron might have performed the subsequent changes in the former input, hence we currently have the former input state rather than the present input. Hence, every consecutive input is termed as a time step.

The formula for employing activation function (tan$h$) is given as.

$$h_t = \tan h(W_{hh} h_{t-1} + W_{xh} x_t). \quad (6)$$

W_{hh} is the weight of the recurring neuron and W_{xh} is the weight of the input neuron. The recurring neuron considers the immediate former states. For longer sequences, the expression could have many such states. When the final state is computed, the next phase is production of the output. The output state is computed using the expression,

$$y_t = W_{hy} h_t, \quad (7)$$

where W_{hy} is the weight at the output layer.

Procedure for Recurrent Neural Networks.

(1) The input x_t is given to the network
(2) Compute the present state utilizing the present input and the former state i.e. we compute h_t
(3) The present h_t turns out as h_{t-1} for the following time step
(4) Several time steps can be carried out as the situation requires and merge the data from all the former states
(5) After completion of the time steps, the last current state is utilized to compute the output y_t
(6) The output is equated with the actual outcome, to check if there is any difference and the error is determined
(7) The error is fed back to the network for updating the weight and the network is trained.

4. Results and Discussion

The Deep Learning algorithm can analyze Cluster 1 given by fuzzy, which contains two defective Thermal crack images, assigns weights or probabilities, and finally outputs the best

match. Hence, the classification task is completed accurately at a faster rate.

The output images of the Proposed method are shown in Figure 3 with the numbering from [1–17]. Image segmentation is generally used to identify objects and boundaries (lines, curves, etc.) in thermal images. More incisively, image segmentation is the procedure of assigning a label to each image pixel, in such a way that pixels with a similar label have certain features such as color, intensity, or texture in common. The result of image segmentation is a group of segments that collectively encompass the full image, or a group of contours extracted from the thermal image. Nearby regions significantly vary with regard to the similar features. Picture 3 represents Edge Detection that possesses a wide range of mathematical operations that intend to detect points in a digital image where the image luminance varies sharply or has discontinuities. The discontinuities correspond to discontinuities in depth, surface orientation, changes in material properties, and fluctuations in scene illumination. Applying an Edge Detection Algorithm to an image may significantly reduce the quantity of information to be processed and may therefore filter out data that may be considered as less relevant, while saving the vital structural properties of an image. Pictures 4 and 5 denote the images with porosity Cluster 1 and Cluster 2, respectively. For a Good image, the Porosity count is 162. Picture 6 denotes the original bad image, in which the defect is indicated by a red marking, which shows the defect in the form of tiny granules close to each other. Picture 7 denotes the segmented image. Segmentation divides an image into distinguishable regions comprising of pixels with common properties. The defect in the segmented image is denoted by the red marking. Picture 8 denotes edge detection being carried out, which is the process of finding out boundaries of an object within an image. The defective region is denoted by red marking. Pictures 9 and 10 denote the image with porosity Cluster 1 and Cluster 2 for metal surface of valves. It clearly shows the porosity defect, which is in the form of closely, spaced granules, whereas the left-hand side of the images seems to be clear. The porosity count in the defective image is found through pixel count and is found to be 414 holes in count. Picture 11 denotes Thermal good image, which is obtained by utilizing Thermal Imaging. Picture 12 denotes the segmented version of the thermal image. Picture 13 denotes Edge Detection. The points at which image luminance varies sharply are typically organized into a set of curved line segments called edges. Pictures 14 and 15 denote the images with porosity Cluster 1 and Cluster 2, respectively. For a good thermal image, the porosity count is 54. Picture 16 denotes the defective thermal image, which is obtained by using Infrared Thermography. Infrared Thermography can identify heat patterns in the infrared wavelength spectrum that are not visible to the naked eye. The defect is indicated by a red marking. Picture 17 denotes the segmented image. Segmentation is the procedure of grouping the pixels of an image in terms of color, texture, and intensity. The right-hand side defective portion of the image, which is indicated by a red marking, is grouped together since they are sharing the same characteristics. Picture 18 denotes the edge detection. It is the process in which image brightness changes in the overall image are analyzed. The defective region in the image is indicated by a red marking. Pictures 19 and 20 denote the porosity defect in the image in terms of Cluster 1 and Cluster 2. Porosity is the presence of cavities in the weld metal caused by the freezing in of gas released from the weld pool as it solidifies. For a Defective thermal image, the porosity count is 72.

In Infrared thermography, each pixel in the image may reflect different degrees of temperature. In some cases, few pixels may reflect the same amount of energy. Hence in Figures 4(a) and 4(c) which denote the thermal images with and without defects, respectively, the difference in reflected energy is represented through different colors. Figures 4(b) and 4(d) denote the Surface plots of the defective and nondefective thermal images, respectively. Surface plot is a graphical version of the two thermal images equivalent to a histogram plot. In Infrared Thermography, defects are more clearly visible and detected easily through algorithms.

The Fuzzy Clustering outputs are denoted in Figure 5 with the numbering from [1–14] and Fuzzy Slicing outputs are denoted in Figure 6 with the numbering from [5, 15–21]. Using fuzzy, it processes the image and forms clusters, totally 4 clusters are formed. Picture 1 comprises of Cluster 1, which contains two Crack images. Picture 2 comprises of Cluster 2, which contains two Porosity images. Picture 3 comprises of Cluster 3, which contains two Corrosion images. Picture 4 comprises of Cluster 4, which contains the Internal Defect image. A similar process is carried out for detecting Porosity, Crack, Internal defects and for classifying them. Picture 17 indicates the index of clusters. Hence, the fuzzy performs slicing of the input image and so five indices or slices are obtained. Picture 18 indicates the boundary, where exactly the defect is located and hence further processing can be performed. Initially, the boundary is not determined. These figures give details on slicing performed by Fuzzy on Defective images. Using fuzzy, 4 clusters are formed. Picture 5 comprises of Cluster 1, which contains two Defective Crack images. The defects in the crack images are indicated by red markings. Picture 6 comprises of Cluster 2, which contains two defective Porosity images. Picture 7 comprises of Cluster 3, which contains two defective Corrosion images. Picture 8 comprises of Cluster 4, which contains the Internal Defect image. A similar process is carried out for detecting defective Porosity, Crack, Internal defects and for classifying them. Picture 19 indicates the fifth cluster group, hence the fuzzy performs slicing of the input image and so five indices or slices are obtained. Picture 20 indicates the boundary, where exactly the defect is located and hence further processing can be performed. Initially, the boundary is not determined. These figures give details on slicing performed by Fuzzy on Thermal images. Using fuzzy, it processes the images and forms clusters, totally 4 clusters are formed. Picture 9 comprises of Cluster 1, which contains two Thermal Crack images. Picture 10 comprises of Cluster 2, which contains two Thermal Porosity images. Picture 11 comprises of Cluster 3, which contains two Thermal Corrosion images. Picture 12 comprises of Cluster 4, which contains the two

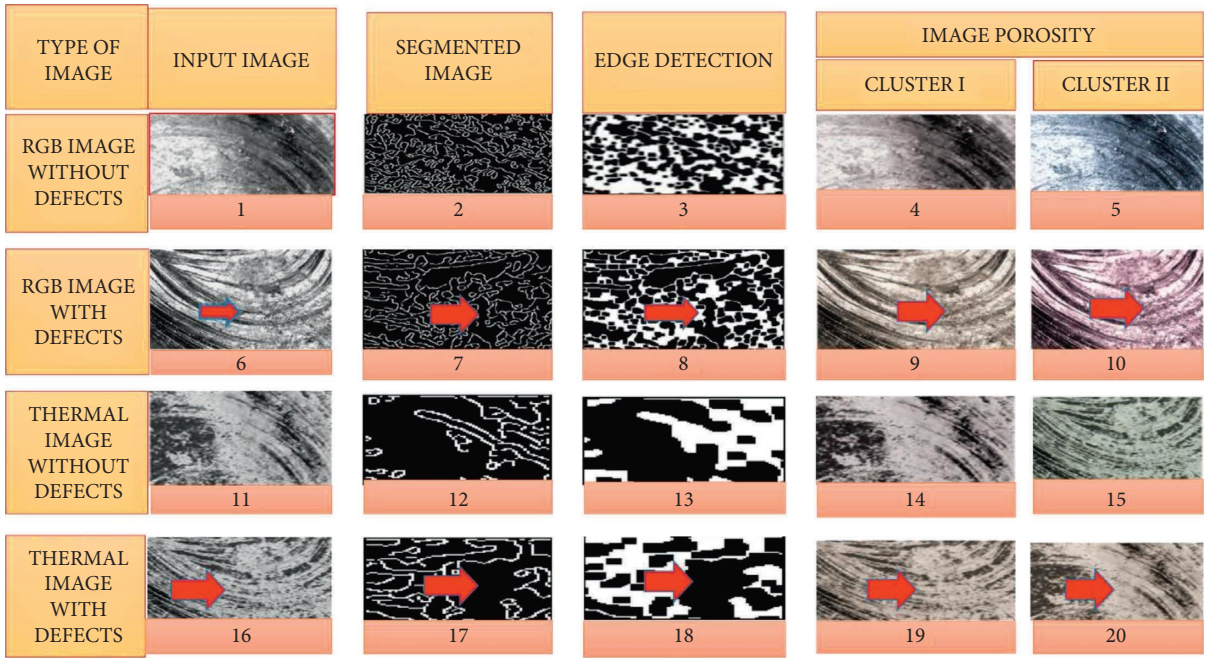

Figure 3: Fuzzy outputs for image porosity using adaptive K-means clustering algorithm.

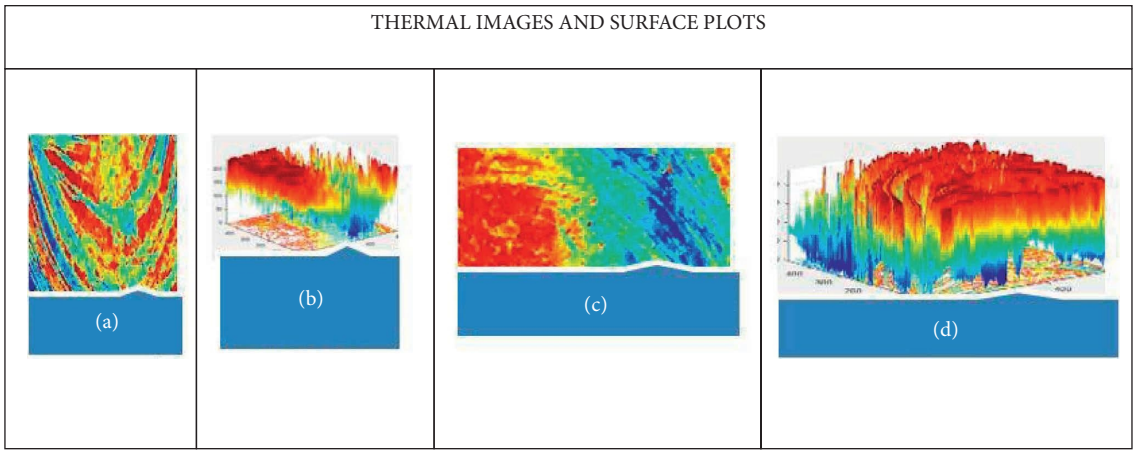

Figure 4: Metal surface and 3D plots. (a) Good thermal image. (b) Good thermal image surface plot. (c) Bad thermal image. (d) Bad thermal image surface plot.

Thermal Internal Defect images. A similar process is carried out for detecting Porosity, Crack, and Internal defects from the Thermal images for classifying defects. Picture 21 indicates the fifth group of pixel clusters, hence the fuzzy performs slicing of the input image and so five indices or slices are obtained. Picture 22 indicates the boundary as to where exactly the defect is located and hence further processing takes place. These figures give details on slicing performed by Fuzzy on defective Thermal images. Using fuzzy, it processes the images and forms clusters, totally 4 clusters are formed. Picture 13 comprises of Cluster 1, which contains two Defective Thermal Crack images. The defects in the Thermal crack images are indicated by red markings. Picture 14 comprises of Cluster 2, which contains two defective Thermal Porosity images. Picture 15 comprises of Cluster 3, which contains two defective Thermal Corrosion images. Picture 16 comprises of Cluster 4, which contains the two Thermal Internal Defect images. A similar process is carried out for detecting defective Thermal Porosity, Crack, Internal defects and also for classifying them. Picture 23 indicates the fifth index cluster, hence the fuzzy performs slicing of the input image and so five indices or slices are obtained. Picture 24 indicates the boundary, where exactly the defect is located and hence further processing takes place.

4.1. Deep Learning. For the Boundary detection and for accurate identification of defects, the Deep Learning algorithm is applied. Furthermore, the Deep Learning algorithm can analyze Cluster 1 given by fuzzy, which contains two defective Thermal crack images, assigns weights or

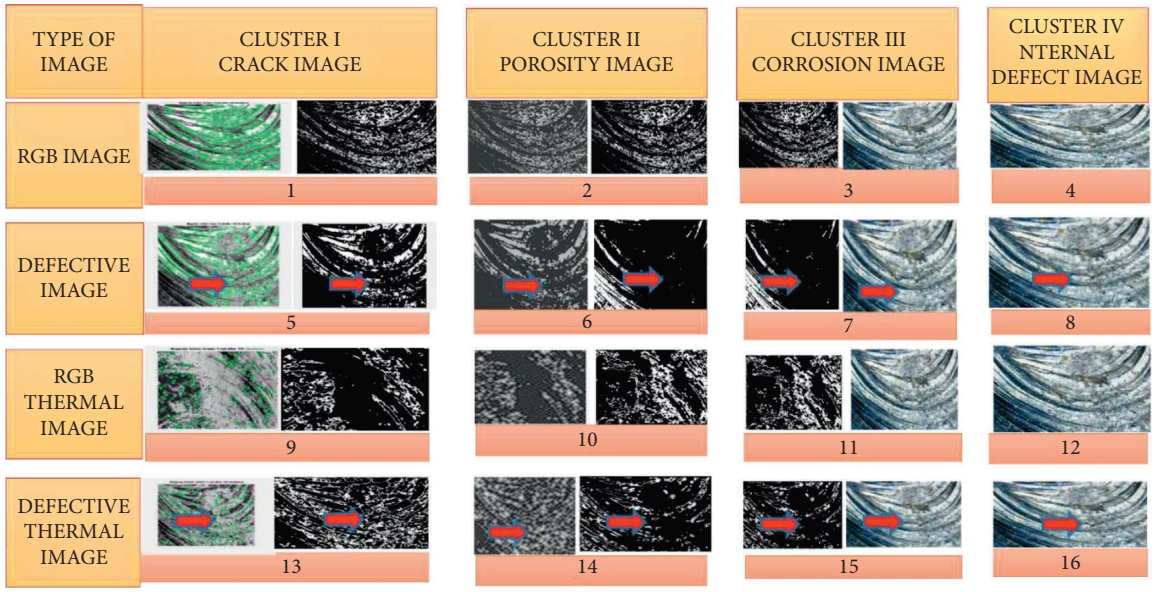

Figure 5: Fuzzy clustering.

probabilities, and finally outputs the best match. Hence, the classification task is completed accurately at a faster rate. The output of the Fuzzy becomes the input to the Deep Learning network. Hence, the Deep Learning network does not have to search for the best match from the universal database but it can search from the fuzzy output. It makes use of ResNet 50 architecture, to perform the classification task. ResNet 50 does the classification by assigning weights or probabilities and determines the best match. It will determine, if the given input image has Porosity, Crack, Corrosion, or Internal defect category. Thus, the classification of defect is perfectly performed by Deep Learning. To enhance the training procedure, a parametric quantity termed center loss is merged with Resnet50.

The center loss function is computed as

$$L_{\text{cen}} = \frac{1}{2}\sum_{i=1}^{N} f(x_i) - c_{yi2}^{2}, \tag{8}$$

where $f(x_i)$ denotes the deep feature, $c_{yi}$is the center of the yth class, and N represents the batch size. The Net Network loss can be obtained by combining softmax loss and center loss:

$$L = L_{cls} + \lambda L_{\text{cen}}, \tag{9}$$

where L_{cls} is softmax loss and λ denotes the weight of center loss. The fuzzification task is performed prior to the application of the concepts of Deep learning, since the role of Fuzzy Algorithm is to simplify the classification task. Deep Learning algorithms are without fuzzy input image then classification accuracy is less. In this case, the Deep Learning algorithm deals with the entire universal collection of images in which the number of images will be more, also there might be irrelevant images being mixed. Deep Learning algorithms perform classification of images from an entire database. Fuzzy algorithms lighten their task by doing the slicing work on the images and then database is given as input for Deep Learning. The Deep Learning algorithms need not analyze the entire collection of images from the universal database, only searches from the selected collection of image database that is rendered by the Fuzzy Algorithm. Hence, this Fuzzy input image lightens the task of the Deep Learning algorithms. After the aid of Fuzzy Algorithm, the Deep Learning algorithms improve the classification time and hence the output is obtained much faster. In addition, since fuzzy has earlier worked on the images and given a select number of images to the Deep learning to perform the classification, there are absolutely no chances of misclassification. Detection and classification of defects that are present in welding thermal images such as Cracks, Porosity, Internaldefects, and Corrosion is the universal collection of image database. This will involve roughly 10,000 images for each type. Hence, Deep Learning algorithms perform the classification task directly from this universal database, which will be tough and will encounter various drawbacks. Hence, to overcome this, we introduced the fuzzy part, which happens prior to Deep learning. This universal collection of Cracks, Porosity, Internal defects, and Corrosion images is fed as input to the Fuzzy block (algorithm). Hence, out of the 10,000 crack images, the Fuzzy Algorithm will filter out and select roughly say 200 relevant images and cluster of crack images. Now, the Deep Learning algorithm will have to work on these 200 selected crack images and perform the best match with the defect that occurred. Similarly, the Fuzzy Algorithm forms clusters for the Porosity, Internal defects, and Corrosion images. Hence, by using Fuzzy Algorithm the output is rendered at a much faster pace and without any misclassification. Figures 7(a) and 7(b) show the denoised crack image and Pixel classified images, respectively. Figures 8(a) and 8(b) show the denoised corrosion image and Pixel classified images, respectively.

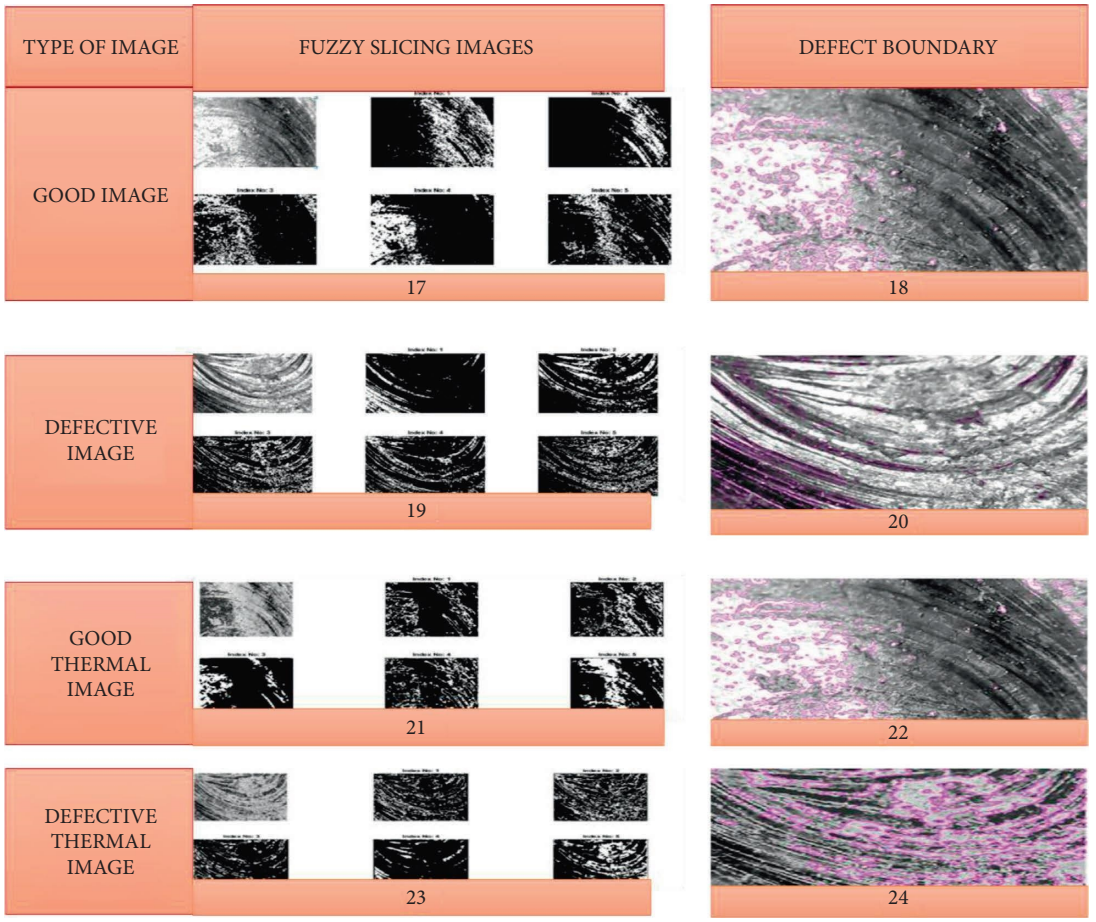

Figure 6: Fuzzy slicing outputs.

4.2. Evaluation Parameters. The efficiency of the proposed technique is verified by utilizing the mentioned parameters in Tables 3 and 4.

4.2.1. Statistical Parameters

(1) True Positive, True Negative, False Positive, and False Negative. A true positive is an effectual operation for prediction of the positive class. Similarly, a true negative is an efficacious method for prediction of the negative class. A false positive is an efficient method for prediction of the false positive class. A false negative is an efficacious operation for prognostication of the false negative class.

(2) Accuracy. Accuracy is the fraction of predictions our method fetched perfectly. Accuracy is given by:

$$\text{Accuracy} = \frac{\text{Number of correct predictions}}{\text{Total no of predictions}}. \tag{10}$$

For binary classification, accuracy is calculated utilizing positives and negatives as given as:

$$\text{Acccuracy} = \frac{(\text{TP} + \text{TN})}{(P + N)}. \tag{11}$$

(3) Precision, Recall. Precision is the count of applicable events among the retrieved events, while Recall (sensitivity) is the count of the total number of applicable events recovered. Precision and Recall depend on an understanding and level of relevance.

$$\begin{aligned} \text{Precision} &= \frac{\text{TP}}{(\text{TP} - \text{FP})}, \\ \text{Recall} &= \frac{\text{TP}}{P}, \\ P &= \text{TP} + \text{FN}, \\ N &= \text{FP} + \text{TN}, \\ \text{FP rate} &= \frac{\text{FP}}{N}, \\ \text{TP rate} &= \frac{\text{TP}}{P}. \end{aligned} \tag{12}$$

The coefficients regard true and false positives, negatives and are applied, even when the classes are of various sizes.

(4) F-measure/F-value. The F_{value} (F-score or F-measure) is a valuation metric for a test's exactitude. To evaluate the score, one views Precision p and Recall r of the test: p is the total

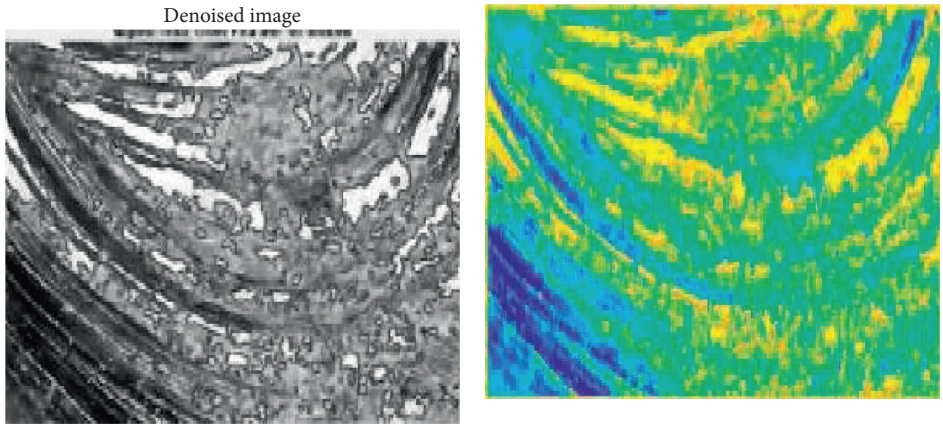

(a) (b)

Figure 7: (a) Denoised crack image. (b) Pixel classified crack image.

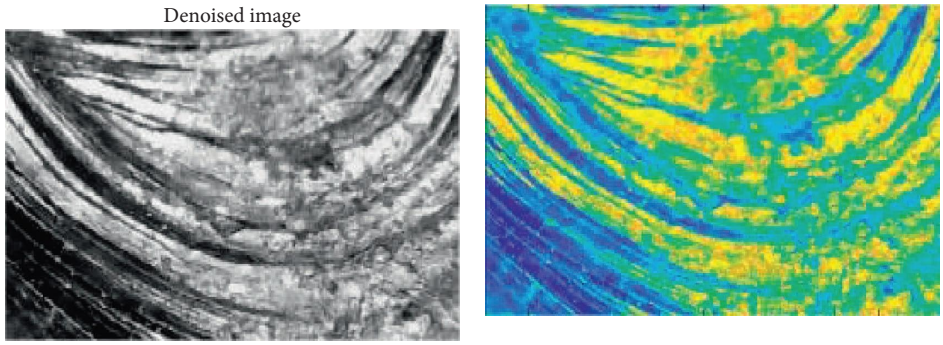

(a) (b)

Figure 8: (a) Denoised corrosion image. (b) Pixel classified corrosion image.

Table 3: Evaluation parameters.

S. No.	Evaluation standards	Fuzzy deep-learning output	
		Pixel classified corrosion image Values	Pixel classified crack image Values
1	Accuracy	0.794	0.8068
2	FN	614	396
3	FP	4020	3952
4	Fprate	0.8627	0.9191
5	Fvalue	0.8814	0.8912
6	Jaccard index	0.788	0.8037
7	MCC	0.1818	0.1301
8	Precision	0.8108	0.8183
9	Recall	0.9656	0.9782
10	TN	640	348
11	TP	17226	17804
12	TPrate	0.9656	0.9782

count of precise positive outcomes fractioned by the total count of positive outcomes the classifier yields and r is the total count of precise positive outcomes fractioned by the total count of all relevant events. The F_1 score is the harmonic average of Precision and Recall, and accomplishes the exact value at 1.

$$F\text{value} = 2 * \left(\frac{\text{precision} * \text{recall}}{\text{precision} + \text{recall}}\right). \tag{13}$$

(5) Mathews Correlation Coefficient (MCC). The MCC is normally a correlation coefficient amidst the observable and predicted binary categorizations, which yield a value ranging

Table 4: Evaluation standards.

S. No.	Parameter	Value
1	MSE	99.41
2	MSE	99.83
3	MSE	107.34
4	PSNR	28.1903302 dB
5	PSNR	28.1722913 dB
6	PSNR	27.8573563 dB
7	SSIM	0.7627
8	LSS	0.0064

from −1 to +1. A coefficient of +1 represents an exact prediction, 0 represents a random prediction, and −1 denotes complete discrepancy between prediction and observation.

$$\mathrm{MCC} = \frac{(\mathrm{TP} * \mathrm{TN} - \mathrm{FP} * \mathrm{FN})}{\sqrt{((\mathrm{TP} + \mathrm{FP}) * (\mathrm{TP} + \mathrm{FN}) * (\mathrm{TN} + \mathrm{FP}) * (\mathrm{TN} + \mathrm{FN}))}}. \tag{14}$$

(6) Jaccard Index. The Jaccard Index, also termed Jaccard similarity coefficient, is a statistical parametric quantity utilized to fetch an in-depth cognition on the similarities within finite sample sets. It is denoted as the intersection of sample sets fractioned by the union of sample sets. The formula for Jaccard Index is as follows.

$$J(A, B) = \frac{|A \cap B|}{A \cup B} = \frac{A \cap B}{|A| + |B| - |A \cap B|}. \tag{15}$$

The Jaccard distance computes dissimilarity within sample sets. The Jaccard distance is got by calculating the Jaccard Index and subtracting from 1, or fractioning the deviations in the intersection of the two sets. Jaccard distance is represented as.

$$D_J = 1 - J(A, B) = \frac{|A \cup B| - |A \cap B|}{A \cup B}. \tag{16}$$

The mean-squared error (MSE) and peak signal-to-noise ratio (PSNR) are employed to ensure the image compression quality. The PSNR ascertains the peak signal-to-noise ratio, in decibels, within two images. This ratio is employed as a quality metric between the original and a compressed image. A higher PSNR value increases the compressed or reconstructed image quality.

$$\mathrm{PSNR} = 10 \log_{10}\left[\frac{R^2}{\mathrm{MSE}}\right], \tag{17}$$

where R is the peak variation in the input image.

Mean-Squared Error (MSE) is the square of differences in the pixel values of the original and compressed images. PSNR represents the measure of peak error. The lesser the MSE value, the lesser the error. What is m, n?

$$\mathrm{MSE} = \frac{1}{\mathrm{MN}} \sum_{M,N} \left[I_1(m, n) - I_2(m, n)\right]^2, \tag{18}$$

where $I_1(m, n)$ is the Original image, $I_2(m, n)$ is the Approximate version, and M, N are the Dimensions of the image.

LSS: LSS descriptors valuate the similarity between images based on matching internal self-similarities. The local "self-similarity descriptor" efficaciously captures the internal self-similarities, valuated enormously over the full image, at different scales, and calculates the local and global geometric aberrations. LSS utilize the detection of objects in images, with no prior knowledge.

5. Conclusion

Fuzzy Deep Learning Algorithm, the output of the Fuzzy Block, is given as input to the Deep Learning block, to simplify the categorization task. The Fuzzy Algorithm performs Slicing operation on the universal collection of image database and renders selective defective images into the Fuzzy image database. Deep Learning Algorithm does not have to classify from the universal image collection and classifies only the selective defective images from the Fuzzy database. This enhances the speed of classification and leads to zero misclassification of defective images. Passive Infrared Thermography's unique feature is that it does not require an external heat source. It rather utilizes the natural infrared radiation coming out of the object. The Dye-Penetrating Test (DPT) outperforms Ultrasonic Testing, in evaluating materials, especially cast iron, through which signals are difficult to be transmitted. If the cast iron Plug valve has a huge grain size, it causes the sound waves to fade, resulting in flaws. The Porosity defects are indicated as closely spaced granules. The Porosity count in a defective thermal image is 72. The clustering results of Cracks, Porosity, Corrosion, and Internal defects are clearly indicated in separate images. The Fuzzy Slicing outputs give details on the slicing operation performed using the index value of $K = 5$. The defect boundary is also indicated as to where exactly is the defect located. The defects are evaluated utilizing parametric quantities such as Precision, Accuracy, Slicing, Jaccard Index, etc. The Parameter values are obtained for each of the 4 defects separately using the corresponding formulas. Hence, this combination of Fuzzy Deep Learning Algorithm renders enhanced efficiency compared to existing algorithms [1].

Data Availability

The data used to support the findings of this study are included within the article.

Conflicts of Interest

The authors declare that they have no conflicts of interest regarding the publication.

References

[1] V. Daniel, A. S. Britto, A. Zimmer, A. L. Koerich, and R. Paludo, "Automatic visual inspection of thermoelectric metal pipes," *Signal, Image and Video Processing*, vol. 13, no. 5, pp. 975–983, 2019.

[2] Z. Zhang, G. Wen, and S. Chen, "Weld image deep learning-based on-line defects detection using convolutional neural

networks for Al alloy in robotic arc welding," *Journal of Manufacturing Processes*, vol. 45, 2019.

[3] S. Chaudhuri, J. Crump, P. A. S. Reed, and B. G. Mellor, "High-resolution 3D weld toe stress analysis and ACPD method for weld toe fatigue crack initiation," *Welding in the World*, vol. 63, no. 6, pp. 1787–1800, 2019.

[4] R. F. Hamade and A. M. R. Baydoun, "Nondestructive detection of defects in friction stir welded lap joints using computed tomography," *Materials & Design*, vol. 162, pp. 10–23, 2019.

[5] M. Jiang, X. Chen, Y. Chen, and W. Tao, "Mitigation of porosity defects in fiber laser welding under low vacuum," *Journal of Materials Processing Technology*, vol. 276, Article ID 116385, 2020.

[6] J. Ye and N. Toyama, "Benchmarking deep learning models for automatic ultrasonic imaging inspection," *IEEE Access*, vol. 9, pp. 36986–36994, 2021.

[7] D. Mery, "Aluminum casting inspection using deep learning: a method based on convolutional neural networks," *Journal of Nondestructive Evaluation*, vol. 39, no. 1, p. 12, 2020.

[8] C. Ajmi, J. Zapata, J. J. Martinez-Alvarez, G. Domenech, and R. Ruiz, "Using deep learning for defect classification on a small weld X-ray image dataset," *Journal of Nondestructive Evaluation*, vol. 39, 2020.

[9] X. Xiao, X. Liu, M. Cheng, and L. Song, "Towards monitoring laser welding process via a coaxial pyrometer," *Journal of Materials Processing Technology*, vol. 277, Article ID 116409, 2020.

[10] K. Schaumberger, M. Beck, J. Saffer et al., "Improving process reliability by means of detection of weld seam irregularities in copper via thermographic process monitoring," *Procedia Manufacturing*, vol. 36, pp. 58–63, 2019.

[11] X. Gao, L. Wang, Z. Chen, Y. Zhang, and D. You, "Process stability analysis and weld formation evaluation during disk laser–mag hybrid welding," *Optics and Lasers in Engineering*, vol. 124, Article ID 105835, 2020.

[12] Z. Lei, B. Li, J. Bi, P. Zhu, W. Lu, and J. Liu, "Influence of the laser thermal effect on the droplet transfer behavior in laser-CMT welding," *Optics & Laser Technology*, vol. 120, Article ID 105728, 2019.

[13] Y. Huang, S. Xu, L. Yang, S. Zhao, Y. liu, and Y. Shi, "Defect detection during laser welding using electrical signals and high-speed photography," *Journal of Materials Processing Technology*, vol. 271, pp. 394–403, 2019.

[14] X. Gao, Y. Li, X. Zhou et al., "Multidirectional magneto-optical imaging system for weld defects inspection," *Optics and Lasers in Engineering*, vol. 124, Article ID 105812, 2020.

[15] X. Xie, Q. Huang, J. Long, Q. Ren, W. Hu, and S. Liu, "A new monitoring method for metal rust removal states in pulsed laser derusting via acoustic emission techniques," *Journal of Materials Processing Technology*, vol. 275, Article ID 116321, 2020.

[16] D. Zhou, J. Liu, Z. Tan, and S. Xu, "Effects of Sn-foil addition on the microstructure and mechanical properties of laser welding joint for dual phase steel and magnesium alloy," *SN Applied Sciences*, vol. 1, no. 7, pp. 694–712, 2019.

[17] Y. R. Choi, S. D. Sun, Q. Liu, M. Brandt, and M. Qian, "Influence of deposition strategy on the microstructure and fatigue properties of laser metal deposited Ti-6Al-4V powder on Ti-6Al-4V substrate," *International Journal of Fatigue*, vol. 130, Article ID 105236, 2020.

[18] D. Bacioiu, G. Melton, M. Papaelias, and R. Shaw, "Automated defect classification of SS304 TIG welding process using visible spectrum camera and machine learning," *NDT & E International*, vol. 107, Article ID 102139, 2019.

[19] U. Shah and X. Liu, "Effects of ultrasonic vibration on resistance spot welding of transformation induced plasticity steel 780 to aluminum alloy AA6061," *Materials & Design*, vol. 182, Article ID 108053, 2019.

[20] N. Nacereddine, A. B. Goumeidane, and D. Ziou, "Unsupervised weld defect classification in radiographic images using multivariate generalized Gaussian mixture model with exact computation of mean and shape parameters," *Computers in Industry*, vol. 108, pp. 132–149, 2019.

[21] J. A. Francis, N. Holtum, S. Olschok et al., "Vacuum laser welding of SA508 steel," *Journal of Materials Processing Technology*, vol. 274, Article ID 116269, 2019.

[22] Y. Zhang, D. You, X. Gao, and S. Katayama, "Online monitoring of welding status based on a DBN model during laser welding," *Engineering*, vol. 5, no. 4, pp. 671–678, 2019.

[23] G. Xu, L. Li, P. Li, Z. Zheng, Q. Hu, and B. Du, "Modeling of keyhole-induced pore formation in laser-arc hybrid welding of aluminum alloy with a horizontal fillet joint," *Journal of Materials Engineering and Performance*, vol. 28, no. 11, pp. 6555–6564, 2019.

[24] J. Y. Son, H. S. Yoon, K. Y. Lee, S. H. Park, and D. S. Shim, "Investigation into high-temperature interfacial strength of heat-resisting alloy deposited by laser melting process," *Metals and Materials International*, vol. 26, no. 3, pp. 384–394, 2019.

[25] U. Reisgen, A. Senger, and S. Olschok, "Electron beam welding in atmosphere of aluminum die casting alloys made of different qualities," *Welding in the World*, vol. 62, no. 6, pp. 1207–1213, 2018.

[26] C. Millon, A. Vanhoye, A. F. Obaton, and J. D. Penot, "Development of laser ultrasonics inspection for online monitoring of additive manufacturing," *Welding in the World*, vol. 62, no. 3, pp. 653–661, 2018.

[27] N. Wu, S. Chen, and J. Xiao, "Wavelet analysis-based expulsion identification in electrode force sensing of resistance spot welding," *Welding in the World*, vol. 62, no. 4, pp. 729–736, 2018.

[28] J. Xie, Y. Ma, W. Xing, L. Zhang, M. Ou, and K. Liu, "Heat-affected zone crack healing in IN939 repaired joints using hot isostatic pressing," *Welding in the World*, vol. 62, no. 3, pp. 471–479, 2018.

[29] Z. Qian, H. Huang, L. Zhao, Q. Ke, and G. Han, "Characterization of spontaneous magnetic signals for residual stress in plasma transferred arc welding process," *Welding in the World*, vol. 63, no. 1, pp. 201–210, 2019.

[30] H. M. Kim, H. R. Yoo, and G. S. Park, "A new design of MFL sensors for self-driving NDT robot to avoid getting stuck in curved underground pipelines," *IEEE Transactions on Magnetics*, vol. 54, no. 11, pp. 1–5, 2018.

[31] W. Hongmin and M. Wang, "Research on detection method of small size weld bead defects based on reluctance measurement," *IEEE Access*, vol. 7, pp. 164068–164079, 2019.

[32] Y. Zhang, X. Gao, D. You, and N. Zhang, "Data-driven detection of laser welding defects based on real-time spectrometer signals," *IEEE Sensors Journal*, vol. 19, no. 20, pp. 9364–9373, 2019.

[33] B. Q. Li and X. Lu, "A biomedical Ti-35Nb-5Ta-7Zr alloy fabricated by powder metallurgy," *Journal of Materials Engineering and Performance*, vol. 28, no. 9, pp. 5616–5624, 2019.